Estimation of nanofiltration solute rejection in reverse osmosis concentrate treatment processes

Sebastian Franzsen[1], Ricky Bonner[1], Jivesh Naidu[1]
Craig Sheridan[2], Geoffrey S. Simate[2]

[1]Miwatek, P/Bag X29, Gallo Manor, 2052, Johannesburg, South Africa, sebastianf@miwatek.co.za
[2]School of Chemical and Mechanical Engineering, University of Witwatersrand, Johannesburg, P/Bag 3,

Abstract

A nanofiltration (NF) model was built in the programming language Python and interfaced with geochemical calculation software PHREEQC COM v3 for the prediction of NF rejection performance in the treatment of reverse osmosis (RO) concentrate. The built NF model is considered to have three industrial applications – (1) tracking in service element degradation in terms of increasing pore radius, decreasing effective active layer thickness and decreasing feed-membrane $\Delta\varphi_{D,m}$, (2) element selection in the design of RO concentrate treatment processes and (3) estimation of unknown solute permeability values by considering the likely ion-pairs and dominant ions that characterises a given aqueous solution.

Keywords: Mine water treatment, brine treatment, nanofiltration modelling

Introduction

Research studies have shown that intermediate chemical demineralisation (CD) of primary reverse osmosis (RO) concentrate followed by secondary RO desalination can substantially improve the volumetric recovery of brackish feed waters (Gabelich et al. 2007, Rahardianto et al. 2007, McCool et al. 2013, Rahardianto et al. 2010, Greenlee et al. 2011).

Different NF elements show substantial performance variation for systems with only slight variation (Artuğ 2007). Phenomenological models and the typical application of single salt (e.g. NaCl, Na_2SO_4, $CaSO_4$, $MgSO_4$ etc.) rejection data are considered inappropriate for NF modelling or NF element selection due to the complexity of the solute transport mechanism.

The DSPM&DE model considers the membrane as having effective pore radius, effective active layer thickness, effective membrane charge density and membrane dielectric constant and is capable of describing the asymptotic concentration gradient at the membrane-solution interfaces (Artuğ 2007, Geraldes and Brites Alves 2008).

The Pitzer aqueous speciation model (pitzer.dat) supplied with PHREEQC can ac-
curately predict thermodynamic properties at high ionic strength for solutions with compositions substantially different from that of seawater (Appelo 2015, Harvie et al. 1984, Pitzer 1981).

The intent of this paper is to present an alternative DSPM & DE model in which (1) the Pitzer activity and osmotic coefficients are determined by incorporating the PHREEQC COM module in the solution algorithm, (2) the aqueous solution is expressed as cation-anion ion pairs with a selected dominant ion for transport and partitioning modelling, and (3) the inclusion of the uncharged specie $SiO2$ provides regression in the absence of electrostatic effects. The model was fitted to data from a pilot scale high recovery RO-CD-NF with recycle to CD process (RO-CD-NF-RCY) and a full-scale RO-NF-CD process. The former process was piloted and the later currently in operation at the Newmont Ahafo mine water treatment plant in Ghana.

Methods

The model domain comprises ten nodes j along the element string feed channel and three distinct regions of solute mass transport at each node presented in Figure 1. The solute transport path and mechanisms through
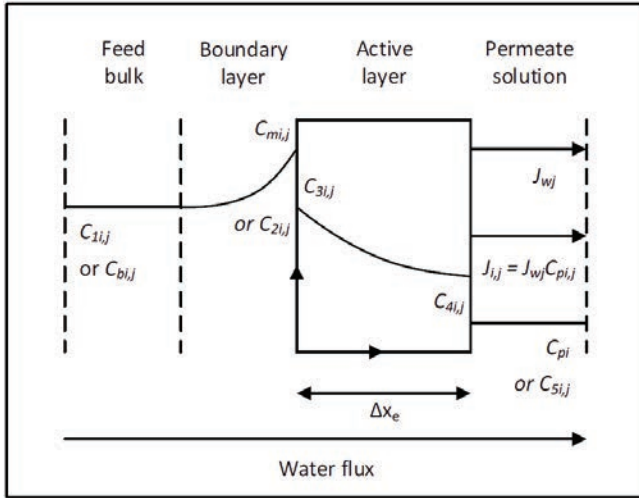
Figure 1 Schematic diagram of the solute concentration profile for each node j

the membrane includes (1) development of a concentration polarisation boundary layer approaching the feed-membrane interface, (2) feed-membrane interface partitioning occurs through steric, Donnan potential and dielectric exclusion, (3) active layer transport and (4) membrane-permeate interface partitioning occurs through steric, Donnan potential and dielectric exclusion.

The aqueous system included H-Na-K-Ca-Mg-OH-HCO$_3$-Cl-SO$_4$-SiO$_2$-CO$_2$ and was arranged into Na$_2$SO$_4$, NaCl, NaHCO$_3$, NaOH, K$_2$SO$_4$, KCl, KHCO$_3$, KOH, CaCl$_2$, CaSO$_4$, Ca(HCO$_3$)$_2$, Ca(OH)$_2$, MgCl$_2$, MgSO$_4$, Mg(HCO$_3$)$_2$, Mg(OH)$_2$, HCl, H$_2$SO$_4$, CO$_2$ and SiO$_2$ ion pairs and molecules.

Equation 1 is the combination of the Mariñas and Urama mass transfer correlation and a correction factor $\in$ for the suction effect generated by permeation through the membrane (Geraldes and Brites Alves 2008, Crittenden et al. 2012). $\in$ is described by semi empirical correlation shown in Equation 2 (Geraldes and Brites Alves 2008).

$$k_{cpi,j} = k_{i,j}\epsilon_{i,j} = \kappa \frac{D_i}{d_H}(Re_j)^{0.5}(Sc_{i,j})^{0.33}.\epsilon_{i,j} \quad \text{Equation 1}$$

$$\in = \emptyset_i + \left(1 + 0.26\emptyset_i^{1.4}\right)^{-1.7} \text{ where } \emptyset_i = \frac{J_{w,j}}{k_{c,i}} \quad \text{Equation 2}$$

The partitioning at the feed-membrane and membrane-permeate interface is described in Equation 3 as a function of three transport resistances – (1) Steric partitioning,

(2) Donnan potential effect and (3) dielectric exclusion (Artuğ 2007). Steric partitioning θ_i expressed in Equation 4, refers to the transport hindrance as a function of solute radii and pore-radii within well-defined cylindrical pores (Labban et al. 2017). The effect of the Donnan potential promotes the transport of counter-ions and hinders the transport of co-ions (Peeters et al. 1998). Dielectric exclusion refers to the reduction in solvation capacity of the pore fluid due to the hydraulics in the confined space of the pores. This barrier to ionic species entering the active layer is referred to as the Born solvation energy barrier ΔW_i and is shown in Equation 5 (Bowen and Welfoot 2002).

$$\frac{\gamma_{ai}c_{ai}}{\gamma_{2i}c_{2i}} = \theta_i.\exp\left(-\frac{z_iF}{R_gT}.\Delta\varphi_D\right).\exp\left(-\frac{\Delta W_{i,Born}}{k_B.T}\right) \quad \text{Equation 3}$$

$$\theta_i = \left(1 - \frac{r_{si}}{r_p}\right)^2 = (1 - \lambda_i)^2 \quad \text{Equation 4}$$

$$\Delta W_{i,Born} = \frac{z_i^2.e^2}{8\pi\epsilon_0 r_{si}}.\left(\frac{1}{\epsilon_p} - \frac{1}{\epsilon_b}\right) \quad \text{Equation 5}$$

Equation 6 represents the solute flux through the membrane using the ENP equation which includes terms for diffusion, electromigration and convection transport (Artuğ 2007, Peeters et al. 1998). Hindrance factors K$_{id}$ and K$_{ic}$ must be applied to the diffusion and convection terms respectively for transport in the active layer (Artuğ 2007).

$$J_{i,j}^{ENP} = -K_{id}D_i\frac{dc_i}{dx} - \frac{z_ic_{i,j}D_{pi}}{R_gT}F\frac{d\varphi}{dx} + K_{ic}c_{i,j}V \quad \text{Equation 6}$$

In this study the active layer transport is reduced to the linear transport between the two inside membrane interfacial concentrations c3 and c4 – refer to Figure 1. To evaluate the $d\varphi/dx$ term, the cation-anion ion pairs were speciated out to individual ions using PHREEQC. Initial estimates of the concentration polarisation layer and permeate concentrations, c2 and c5 respectively, are determined through Equations 7 to 11.

Solution algorithm for NF model

Step 1 is to separate the feed solution into cation-anion ion pairs, specify the element properties, model parameters, process inputs and regression parameters. The parameters specific to each of the ion pairs and the individual ions are calculated – stokes radius, stokes radius to membrane pore radius, convection hindrance factor, diffusion hindrance factor and Born solvation energy barrier. Table 1 lists the input parameters for the calibration cases of the RO-NF-CD and RO-CD-NF-RCY processes.

Step 2 is to estimate the hydraulic parameters, water flux, solute flux and outside membrane concentrations (c_1, c_2 and c_5) to enable the evaluation of the ENP and partitioning equations (Equations 3 and 6 respectively). Equation 7 is the solute flux as each stage j expressed in terms of a phenomenological constant that is generalised for each of the cation-anion ion pairs. Equation 8 is the membrane water flux equation with the

membrane specific water permeability constant A.

$$J_{i,j} = B_i\left(\beta_{i,j}c_{bi,j} - c_{pi,j}\right) \qquad \text{Equation 7}$$

$$J_{w,j} = A\left[\left(P_{b,j} - P_p\right) - \left(\pi_{m,j} - \pi_{p,j}\right)\right] \quad \text{Equation 8}$$

The concentration polarisation at each node, expressed in terms of water flux, mass transfer coefficient and rejection and generalised for each specie, is shown in Equation 9 (Crittenden et al. 2012). Equation 10 is the definition of the solute flux generalised for each specie and the permeate concentration substituted with the equivalent in terms of solute rejection and feed bulk concentration (Crittenden et al. 2012).

$$\beta_{i,j} = e^{J_{w,j}/k_{cpi,j}}.r_{i,j} + \left(1 - r_{i,j}\right) \qquad \text{Equation 9}$$

$$J_{i,j} = J_{w,j}c_{pi,j} = J_{w,j}(1 - r_i)c_{bi,j} \qquad \text{Equation 10}$$

Setting Equation 10 equal to Equation 7 and substituting Equation 9 leads to an equation that relates the solute rejection, solute permeability constant, concentration polarisation mass transfer coefficient and the water flux – Equation 11:

$$r_{i,j} = \left[B_i e^{J_w/k_{cpi,j}} + J_{w,j}\right]^{-1}.J_{w,j} \qquad \text{Equation 11}$$

The solver iterates through the nodes several times and utilises the Newton method from the *Scipy.Optimize* package to solve for the water flux at each node that satisfies the solute rejections from Equation 11 at the

Table 1. Model input parameters for calibration case

Model input parameters	Unit	RO-NF-CD	RO-CD-NF-RCY
Element		MDS NF 8040	MDS NF 4040T
Design volumetric recovery	%	50	50
Membrane surface area	m²	33.1	7.3
Feed pressure	kPag	1065	1750
Operating temperature	°C	30	30
Feed flow rate	m³/h	5.1	1.9
Elements per string		5	8
Nodes per element string		10	10
Feed spacer thickness	Mil	31	31

specified feed pressure. This iterative strategy, as opposed to a simultaneous solution algorithm, was used to incorporate the PHRE-EQC COM module.

Step 3 is to evaluate the c3 and c4 using Equation 3. The $d\varphi/dx$ term must be determined to calculate the solute flux according to the ENP Equation 6. The ratio of the solute flux determined by the ENP Equation 9 and the solute permeability constant in Equation 7 are used to adjust the solute permeability constant of each cation-anion ion pair. The solute permeability constant for the next solver iteration is determined by using Equation 12

Step 4 checks the convergence criteria and returns the solver to step 2 until convergence is achieved. The final cation-anion ion pairs are speciated out in PHREEQC and the overall rejection of individual ions reported.

Results and Discussion

The results of the regression of key parameters to operational data are shown in Table 2 and the comparison of rejection performance between the model and the analytical results are shown in Table 3. The regression of the pore radius and effective active layer thickness was constrained to yield close agreement with rejection of uncharged species SiO_2. This technique is useful as the rejection of SiO_2 is not subject to the electrostatic effects at the system pH.

The dominant ions were assigned for a negative feed-membrane Donnan potential, since (1) ion pairs with divalent anion has the anion as dominant as the repulsion from the feed-membrane interface appeared dominant, (2) ion pairs with monovalent anion and cation has the cation as dominant as the attraction to the feed-membrane interface appeared dominant, (3) pairs with divalent cation and monovalent anion had the divalent cation as dominant as the attraction to the feed-membrane interface appeared dominant and (4) pairs with divalent cation and divalent anion had the divalent anion as dominant as the repulsion from the feed-membrane interface appeared dominant.

$$B_{i,j} = J_{i,j}^{ENP} \cdot \left[\beta_{i,j} c_{bi,j} - c_{pi,j}\right]^{-1} \text{ and } B_i = \overline{B}_{i,j} \qquad \text{Equation 12}$$

The effect of membrane pore dielectric constant ε_{pore} and feed-membrane Donnan potentials $\Delta\varphi_{D,m}$ on rejection performance of the MDS NF 8040 elements in the RO-NF-CD process are shown in Figures 2 and 3. Reducing ε_pore increases the Born solvation energy barrier ΔW_i at the feed-membrane interface and hence the rejection performance of all charged species is improved.

The uncharged specie SiO_2 is not affected by changes in $\Delta\varphi_{D,M}$ or ε_{pore}. Increasing the negative $\Delta\varphi_{D,M}$ increases the repulsion of co-ions and the attraction of counter-ions. For higher negative $\Delta\varphi_{D,M}$, SO_4 rejection increases due to co-ion repulsion, Ca and Mg rejection decreases due to counter-ion attraction, HCO_3 and Cl rejection decreases due to counter-ion attraction (dominant ions are cations for monovalent anions).

Table 2. Regression results for RO-NF-CD full scale and RO-CD-NF-RCY pilot processes

Calibration case regression results		Unit	RO-NF-CD FULL SCALE	RO-CD-NF w/ recycle PILOT
Element	r_{pore}		MDS NF 8040	MDS NF 4040T
Pore radius	Δx_e	nm	0.57	0.535
Active layer thickness	ε_{pore}	μm	0.3	0.3
Membrane dielectric constant	A		39.5	39.5
Water permeability constant	$\Delta\phi_{D,m}$	ms⁻¹bar-1	5.28E-07	7.5E-07
Feed-membrane potential	$\Delta\phi_{D,p}$	mV	- 30	- 4.5
Membrane-permeate potential		mV	+ 20	+ 0.5
Permeate pH [model / (analytical)]			7.6 / (7.7)	5.7 / (5.7)
Feed pH [model / (analytical)]			7.7 / (7.9)	5.9 / (5.9)

Table 3. Comparison of ion rejections determined by the model and the analytical results from SGS

Date	Data	Na rej %	K rej %	SO$_4$ rej %	Ca rej %	Mg rej %	HCO$_3$ rej %	Cl rej %	SiO$_2$ rej %
RO-NF-CD	Model	25.1	25.1	99.4	82.7	94.1	26.0	3.1	6.1
FULL SCALE	SGS	21.0	23.5	99.6	86.7	94.4		0.3	5.9
RO-CD-NF-RCY	Model	96.4	96.4	99.2	99.2	99.3	20.5	0.0	11.7
PILOT	SGS	96.4	96.8	99.1	99.6	99.1		< 0	13.5
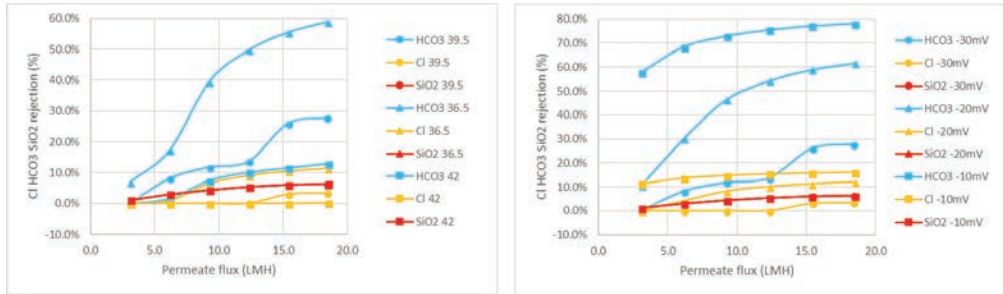
Figure 2 *The effect of membrane pore dielectric constant and feed-membrane Donnan potentials on the HCO3, Cl and SiO2 rejection performance of the MDS NF 8040 elements in the RO-NF-CD process*
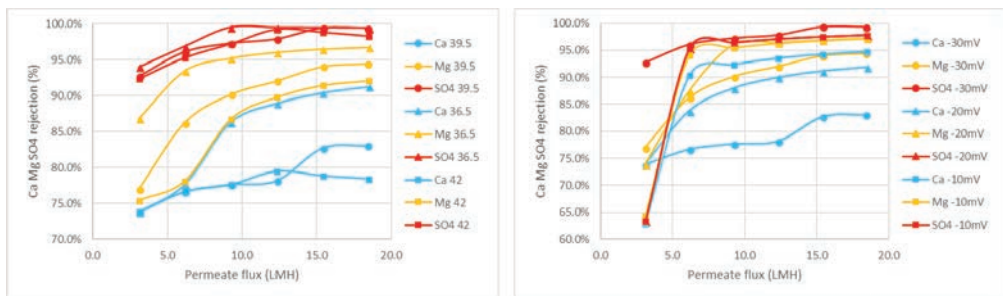
Figure 3 *The effect of membrane pore dielectric constant and feed-membrane Donnan potentials on the Ca, Mg and SO4 rejection performance of the MDS NF 8040 elements in the RO-NF-CD process*

Conclusions

The fundamental differences between this work and other ENP and DSPM & DE studies are (1) the arrangement of the ions into cation-anion ion pairs with a representative dominant ion, (2) the assignment of $\Delta\varphi_{D,m}$ and $\Delta\varphi_{D,p}$ as input values, and (3) the omission of the charge offset -C_X. The built NF model can match the rejection performance of the MDS elements in the RO-NF-CD and RO-CD-NF-RCY processes with resulting $\Delta\varphi_{D,m}$ and $\Delta\varphi_{D,p}$ values and membrane pore dielectric constant (39.5 for both NF elements) that are within the expected ranges for Polyamide membrane active layers. It is recommended that the NF model is fitted to

additional operational data and the fitted parameters, $\Delta\varphi_{D,m}$, $\Delta\varphi_{D,p}$ and ε_{pore}, compared to fitted parameters of a conventional ENP and DSPM & DE model to better understand the limitations and advantages of the ion pairing with dominant ion feature of the built NF model.

The built NF model is considered to have three industrial applications – (1) tracking in service element degradation in terms of increasing pore radius, decreasing effective active layer thickness and decreasing feed-membrane $\Delta\varphi_{D,m}$, (2) element selection in the design of RO-NF-CD and RO-NF-CD-RCY processes and (3) estimation of unknown solute B values by considering the likely ion-

pairs and dominant ions that it may form for a given solution type. The interface with the PHREEQC COM module for the calculation of Pitzer activity and osmotic coefficients is considered an advantage for fitting of high ionic strength applications.

Acknowledgements

References

Gabelich, C.J., Williams, M.D., Rahardianto, A., Franklin, J.C. and Cohen, Y. (2007) High-recovery reverse osmosis desalination using intermediate chemical demineralization. Journal of Membrane Science 301(1–2), 131-141.

Rahardianto, A., Gao, J., Gabelich, C.J., Williams, M.D. and Cohen, Y. (2007) High recovery membrane desalting of low-salinity brackish water: Integration of accelerated precipitation softening with membrane RO. Journal of Membrane Science 289(1–2), 123-137.

McCool, B.C., Rahardianto, A., Faria, J.I. and Cohen, Y. (2013) Evaluation of chemically-enhanced seeded precipitation of RO concentrate for high recovery desalting of high salinity brackish water. Desalination 317, 116-126.

Rahardianto, A., McCool, B.C. and Cohen, Y. (2010) Accelerated desupersaturation of reverse osmosis concentrate by chemically-enhanced seeded precipitation. Desalination 264(3), 256-267.

Greenlee, L.F., Testa, F., Lawler, D.F., Freeman, B.D. and Moulin, P. (2011) Effect of antiscalant degradation on salt precipitation and solid/liquid separation of RO concentrate. Journal of Membrane Science 366(1-2), 48-61.

Artuğ, G. (2007) Modelling and Simulation of Nanofiltration Membranes, Cuvillier.

Geraldes, V. and Brites Alves, A.M. (2008) Computer program for simulation of mass transport in nanofiltration membranes. Journal of Membrane Science 321(2), 172-182.

Appelo, C.A.J. (2015) Principles, caveats and improvements in databases for calculating hydrogeochemical reactions in saline waters from 0 to 200°C and 1 to 1000atm. Applied Geochemistry 55, 62-71.

Harvie, C.E., Møller, N. and Weare, J.H. (1984) The prediction of mineral solubilities in natural waters: The Na-K-Mg-Ca-H-Cl-SO4-OH-HCO3-CO3-CO2-H2O system to high ionic strengths at 25°C. Geochimica et Cosmochimica Acta 48(4), 723-751.

Pitzer, K.S. (1981) Characteristics of very concentrated aqueous solutions. Physics and Chemistry of the Earth 13–14, 249-272.

Crittenden, J.C., Harza, M.W., Trussell, R.R. and Hand, D.W. (2012) MWH's Water Treatment: Principles and Design, Wiley.

Labban, O., Liu, C., Chong, T.H. and Lienhard, J.H. (2017) Fundamentals of low-pressure nanofiltration: Membrane characterization, modeling, and understanding the multi-ionic interactions in water softening. Journal of Membrane Science 521, 18-32.

Peeters, J.M.M., Boom, J.P., Mulder, M.H.V. and Strathmann, H. (1998) Retention measurements of nanofiltration membranes with electrolyte solutions. Journal of Membrane Science 145(2), 199-209.

Bowen, W.R. and Welfoot, J.S. (2002) Modelling the performance of membrane nanofiltration—critical assessment and model development. Chemical Engineering Science 57, 1121-1137.